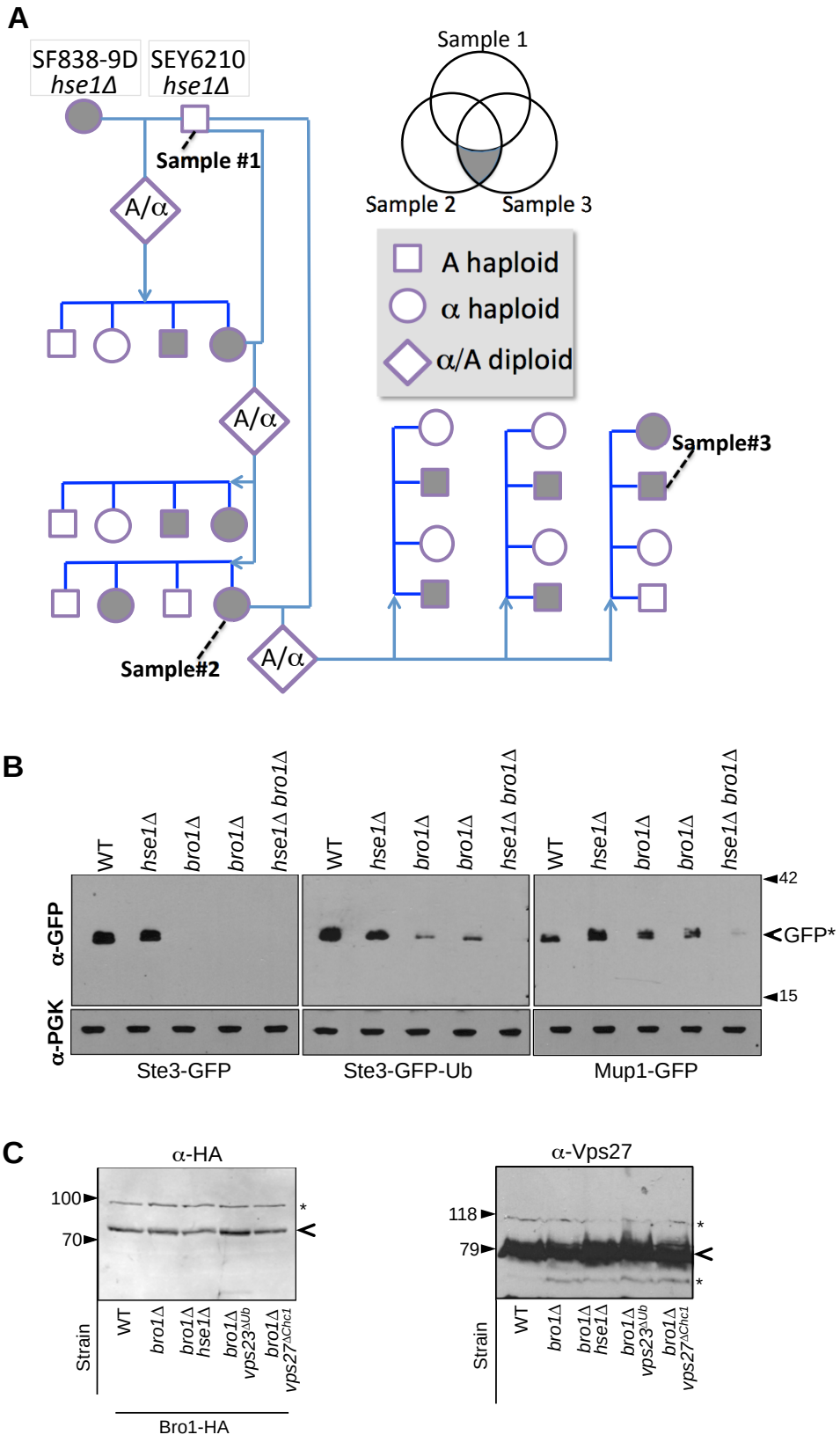
A
SF838-9D
hse1Δ
SEY6210
hse1Δ
Sample #1
A/α
A/α
Sample#2
A/α
Sample 1
Sample 2
Sample 3
A haploid
α haploid
α/A diploid
Sample#3
B
WT
hse1Δ
bro1Δ
bro1Δ
hse1Δ bro1Δ
WT
hse1Δ
bro1Δ
bro1Δ
hse1Δ bro1Δ
WT
hse1Δ
bro1Δ
bro1Δ
hse1Δ bro1Δ
α-GFP
α-PGK
42
GFP*
15
Ste3-GFP
Ste3-GFP-Ub
Mup1-GFP
C
α-HA
100
70
*
Strain
WT
bro1Δ
bro1Δ hse1Δ
bro1Δ vps23ΔUb
bro1Δ vps27ΔChc1
Bro1-HA
α-Vps27
118
79
*
*
Strain
WT
bro1Δ
bro1Δ hse1Δ
bro1Δ vps23ΔUb
bro1Δ vps27ΔChc1

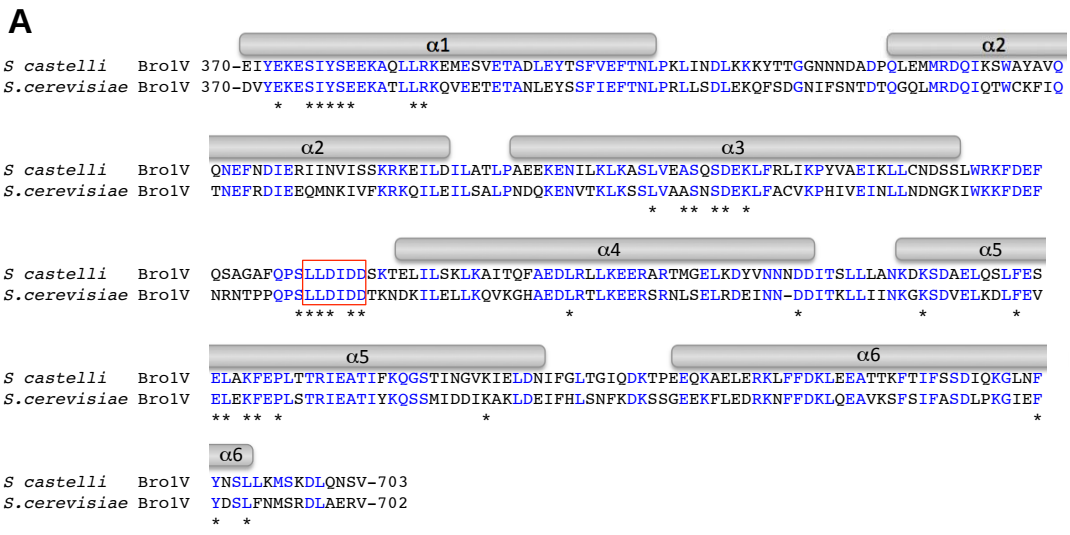
A
α1
α2
S castelli Bro1V 370-EIYEKESIYSEEKAQLLRKEMESVETADLEYTSFVEFTNLPKLINDLKKKYTTGGNNNDADPQLEMMRDQIKSWAYAVQ
S.cerevisiae Bro1V 370-DVYEKESIYSEEKATLLRKQVEETETANLEYSSFIEFTNLPRLLSDLEKQFSDGNIFSNTDTQGQLMRDQIQTWCKFIQ
α2
α3
S castelli Bro1V QNEFNDIERIINVISSKRKEILDILATLPAEEKENILKLKASLVEASQSDEKLFRLIKPYVAEIKLLCNDSSLWRKFDEF
S.cerevisiae Bro1V TNEFRDIEEQMNKIVFKRKQILEILSALPNDQKENVTKLKSSLVAASNSDEKLFACVKPHIVEINLLNDNGKIWKKFDEF
α4
α5
S castelli Bro1V QSAGAFQPSLLDIDDSKTELILSKLKAITQFAEDLRLLKEERARTMGELKDYVNNNDDITSLLLANKDKSDAELQSLFES
S.cerevisiae Bro1V NRNTPPQPSLLDIDDTKNDKILELLKQVKGHAEDLRTLKEERSRNLSELRDEINN-DDITKLLIINKGKSDVELKDLFEV
α5
α6
S castelli Bro1V ELAKFEPLTTRIEATIFKQGSTINGVKIELDNIFGLTGIQDKTPEEQKAELERKLFFDKLEEATTKFTIFSSDIQKGLNF
S.cerevisiae Bro1V ELEKFEPLSTRIEATIYKQSSMIDDIKAKLDEIFHLSNFKDKSSGEEKFLEDRKNFFDKLQEAVKSFSIFASDLPKGIEF
α6
S castelli Bro1V YNSLLKMSKDLQNSV-703
S.cerevisiae Bro1V YDSLFNMSRDLAERV-702
B
Arm 1
Arm 2
α1
α2
α4
α3
α5
α6
QPSLLDIDDTK Saccharomyces cerevisiae
QPSLLDIDDSK Saccharomyces castellii
KQSLLDIDDSK Candida glabrata
TESLLDIDDTE Vanderwaltozyma polyspora
TPDLLDLDHSK Ashbya gossypii
EISLLDIDDSQ Debaryomyces hansenii
ELSLLDMDETQ Meyerozyma guilliermondii
EVSLLDMDDAQ Clavispora lusitaniae
EISLLDIDDNN Candida dubliniensis
EVSLLDIDDRS Pichia pastoris
TVSLLDLDDEE Cryptococcus gattii
SESLIDLDFSQ Yarrowia lipolytica
C
260
135
95
72
52
42
34
α-HA
Vector
MIT-UL36
Bro1-UL36
B1D-UL36
His3-UL36
Bro1-Ubp7
α-PGK

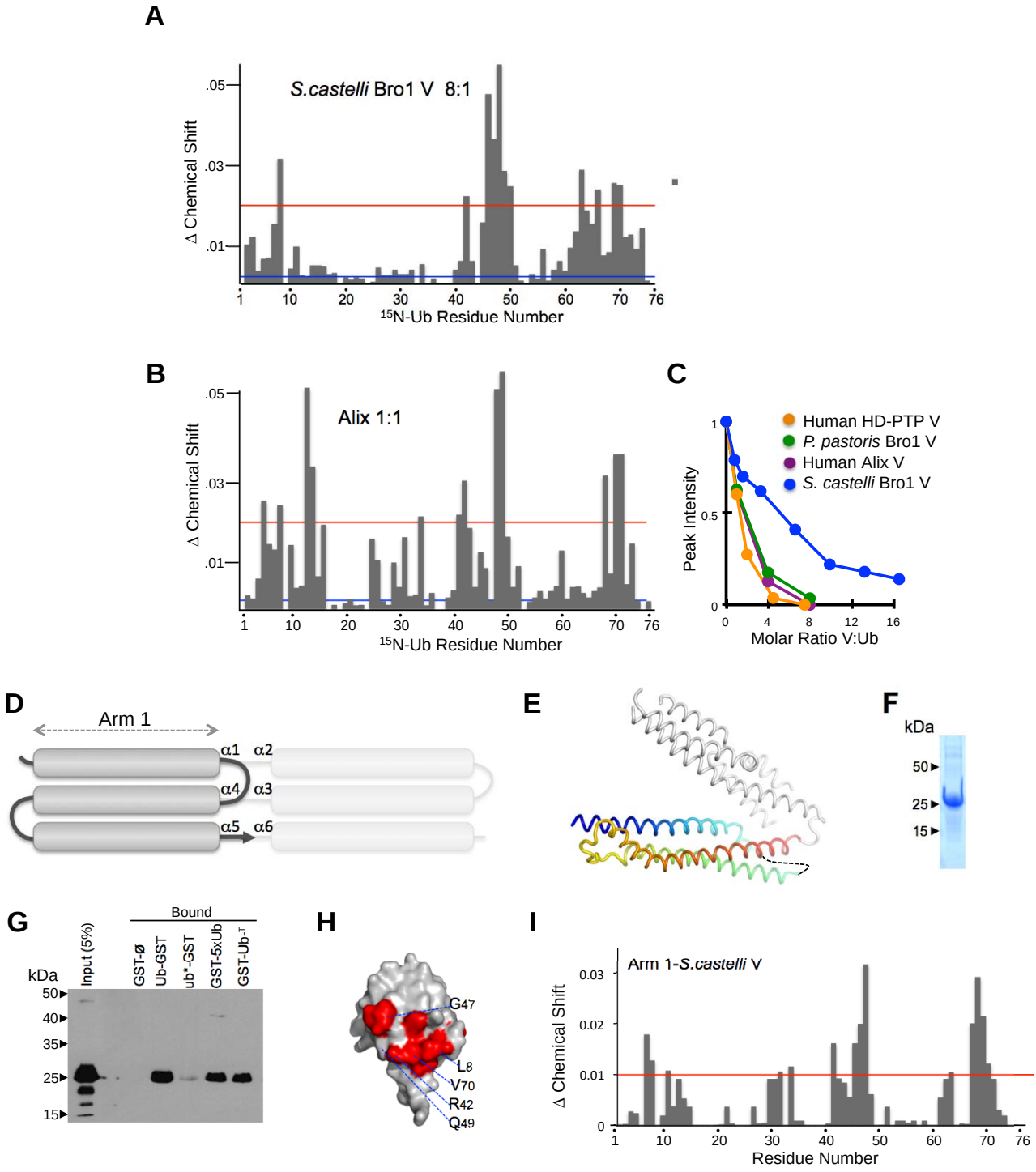
A
S.castelli Bro1 V 8:1
Δ Chemical Shift
.05
.03
.01
1 10 20 30 40 50 60 70 76
15N-Ub Residue Number
B
Alix 1:1
Δ Chemical Shift
15N-Ub Residue Number
C
Human HD-PTP V
P. pastoris Bro1 V
Human Alix V
S. castelli Bro1 V
Peak Intensity
Molar Ratio V:Ub
D
Arm 1
α1 α2
α4 α3
α5 α6
E
F
kDa
50
25
15
G
Bound
Input (5%)
GST-ø
Ub-GST
ub*-GST
GST-5xUb
GST-Ub-T
kDa
50
40
35
25
15
H
G47
L8
V70
R42
Q49
I
Arm 1-S.castelli V
Δ Chemical Shift
0.03
0.02
0.01
0
1 10 20 30 40 50 60 70 76
Residue Number

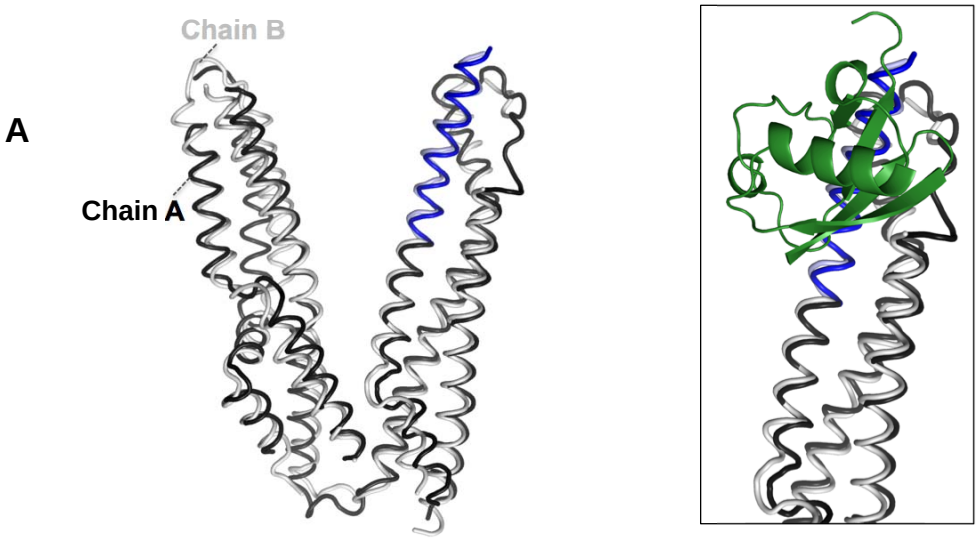
A
Chain B
Chain A

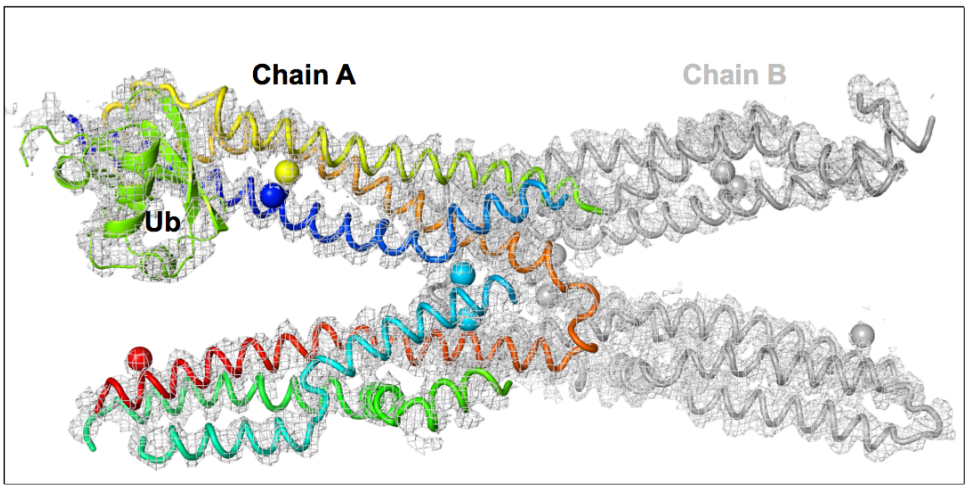
B
Chain A
Chain B
Ub

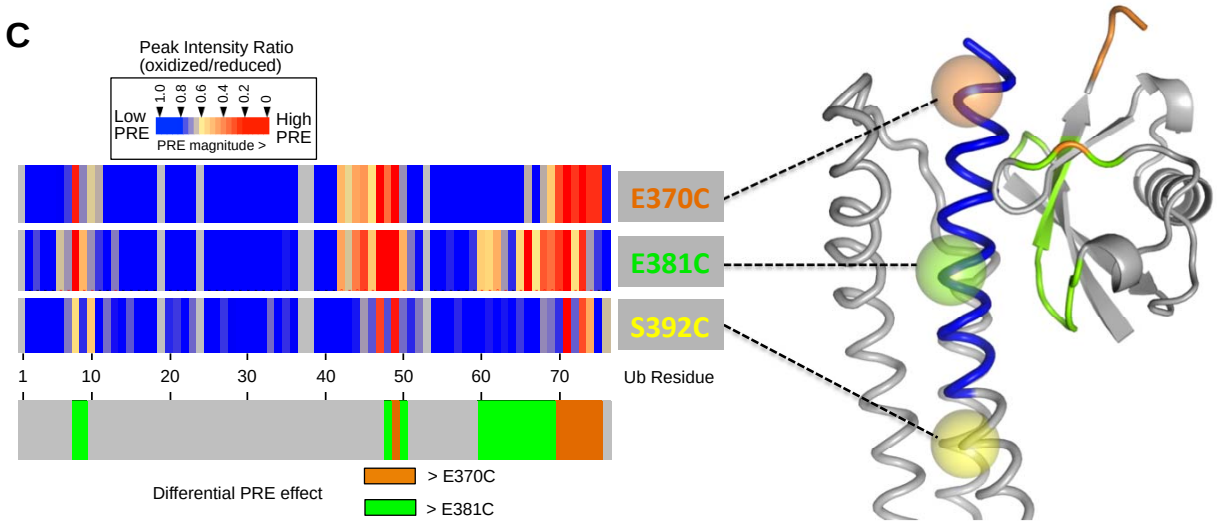
C
Peak Intensity Ratio
(oxidized/reduced)
1.0
0.8
0.6
0.4
0.2
0
Low PRE
High PRE
PRE magnitude >
E370C
E381C
S392C
1
10
20
30
40
50
60
70
Ub Residue
Differential PRE effect
> E370C
> E381C

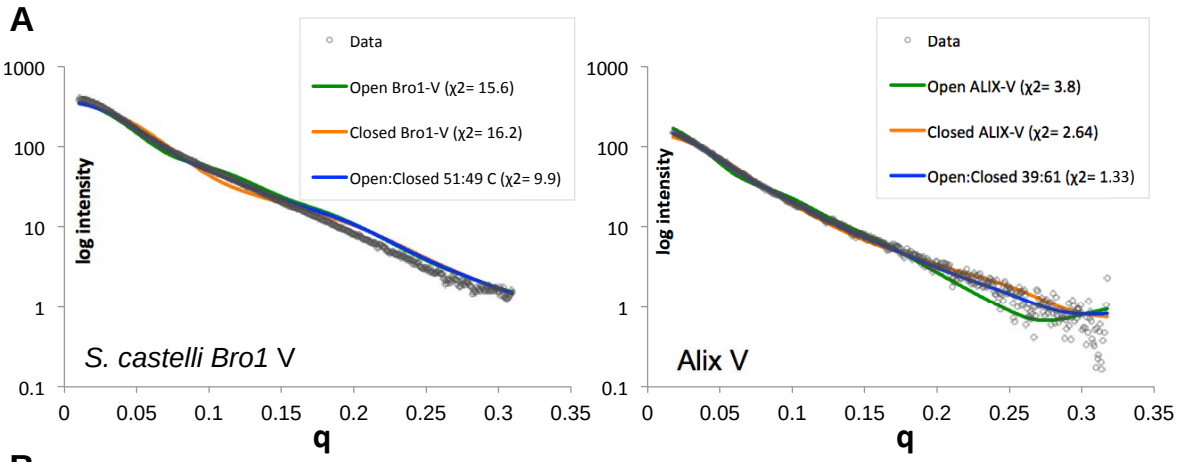

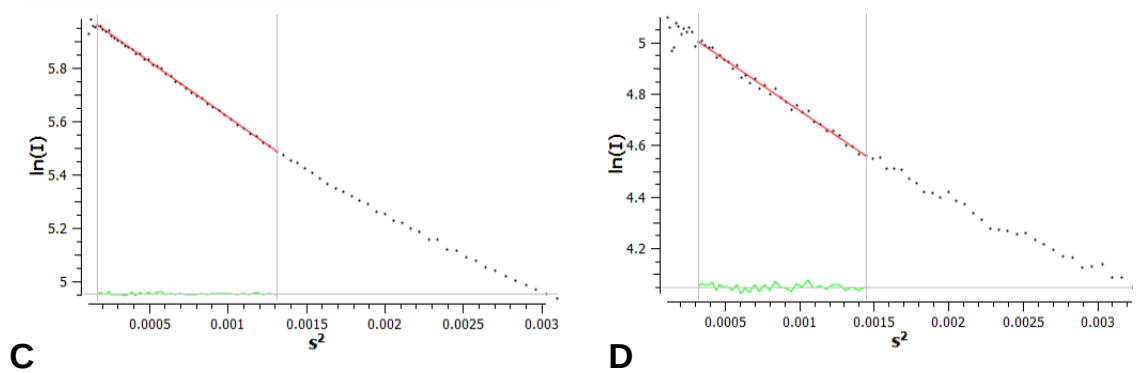

C

Gel Filtration: Superdex 75 column
Alix V at 25°C

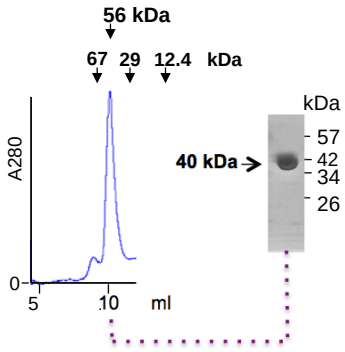

D

Gel Filtration: Superdex 75 column
Bro1 V @ 10.4 mg/ml, at 25°C

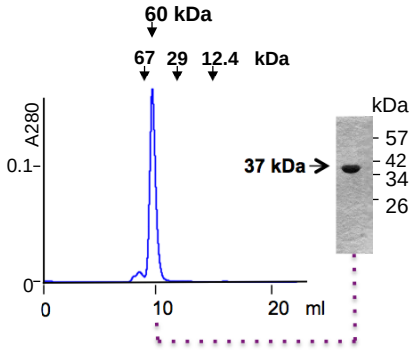

E

	Bro1 V	Alix V
DLS		
Radius (nm)	3.5+0.0	3.3+0.02
%Pd	3.3+0.1	8.6+0.9
MW (kDa)	**62.5+0.6**	**55.1+0.7**
GelFiltration		
MW (kDa)	**60**	**56**
SLS		
MW (kDa)	**34.1+0.05**	**36.7+0.3**
Predicted		
(MW (kDa)	**36.0**	**40.6**

F

Gel Filtration: Superdex 75 column
Cleaved Bro1V^{TEV} @ 10 mg/ml, at 25°C

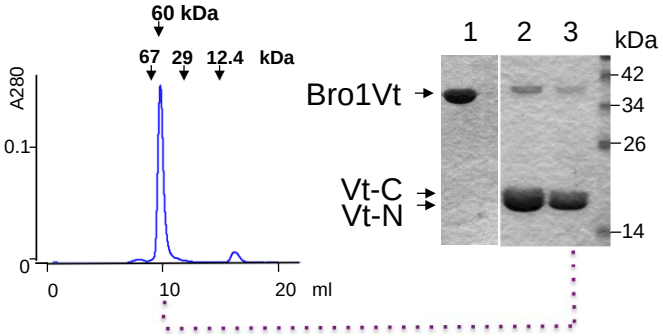

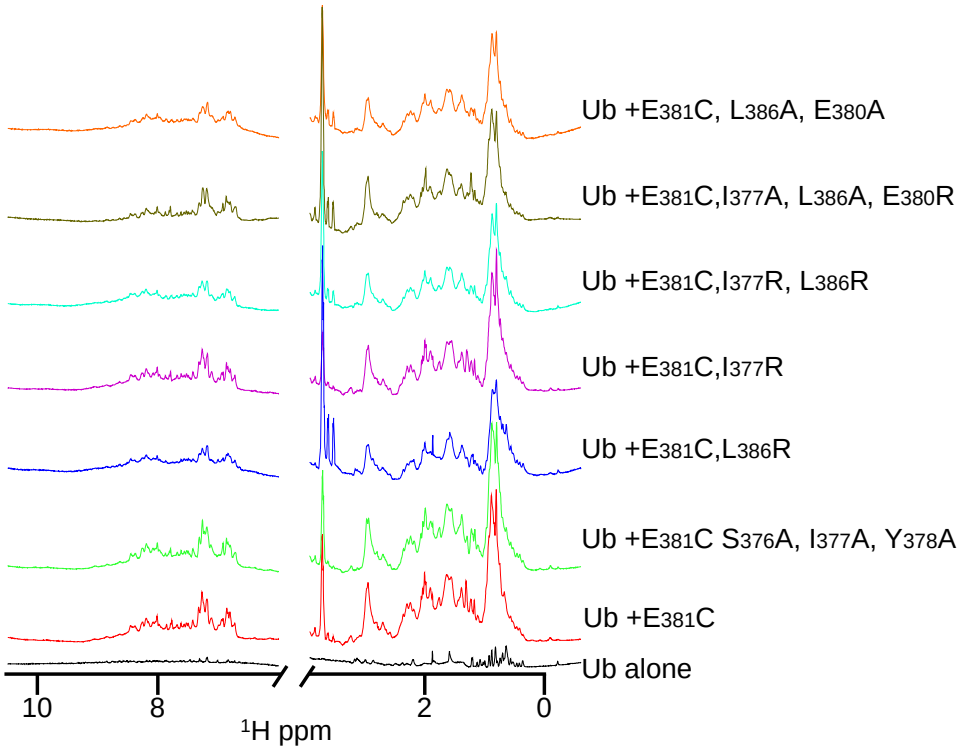
Ub +E381C, L386A, E380A
Ub +E381C,I377A, L386A, E380R
Ub +E381C,I377R, L386R
Ub +E381C,I377R
Ub +E381C,L386R
Ub +E381C S376A, I377A, Y378A
Ub +E381C
Ub alone
10
8
2
0
1H ppm

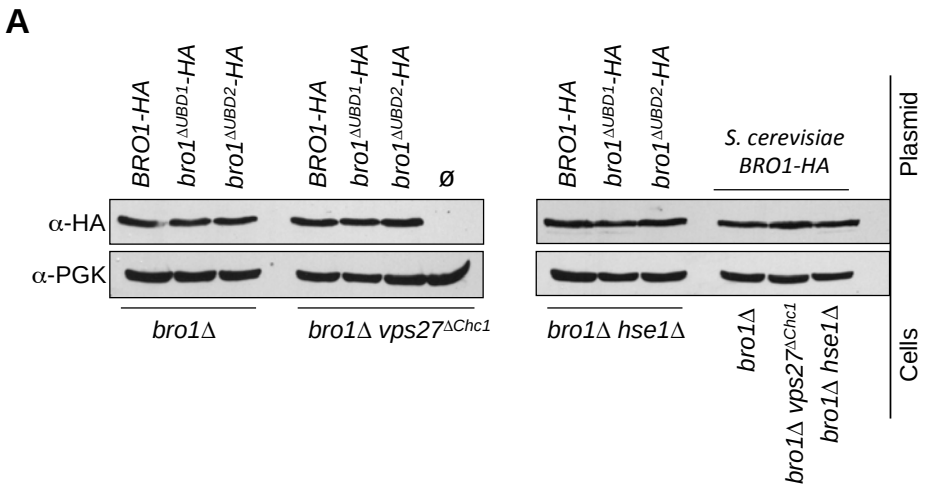
A
BRO1-HA
bro1ΔUBD1-HA
bro1ΔUBD2-HA
BRO1-HA
bro1ΔUBD1-HA
bro1ΔUBD2-HA
ø
BRO1-HA
bro1ΔUBD1-HA
bro1ΔUBD2-HA
S. cerevisiae BRO1-HA
Plasmid
α-HA
α-PGK
bro1Δ
bro1Δ vps27ΔChc1
bro1Δ hse1Δ
bro1Δ
bro1Δ vps27ΔChc1
bro1Δ hse1Δ
Cells

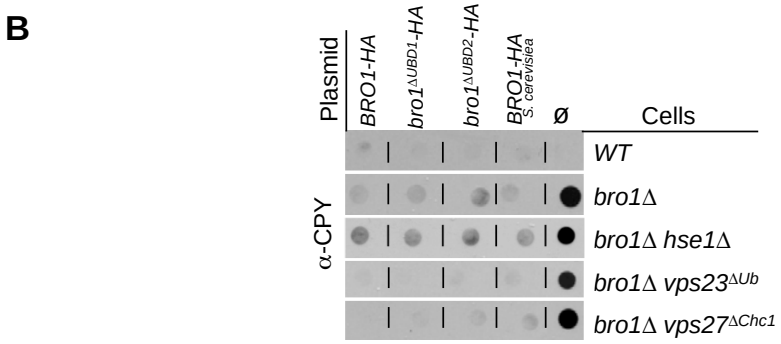
B
Plasmid
BRO1-HA
bro1ΔUBD1-HA
bro1ΔUBD2-HA
BRO1-HA S. cerevisiea
ø
Cells
α-CPY
WT
bro1Δ
bro1Δ hse1Δ
bro1Δ vps23ΔUb
bro1Δ vps27ΔChc1

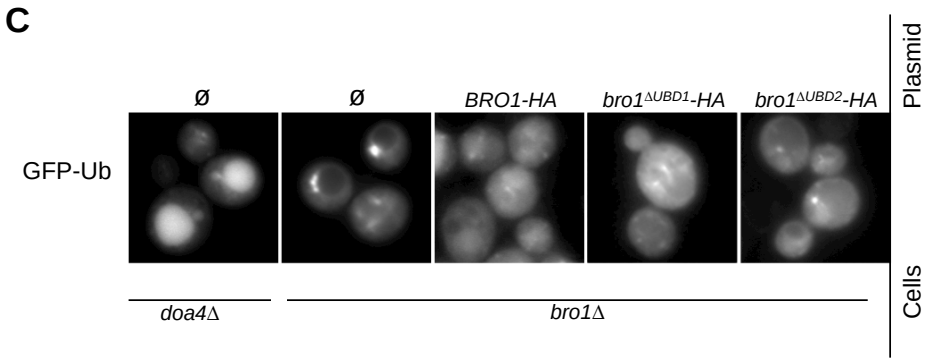
C
ø
ø
BRO1-HA
bro1ΔUBD1-HA
bro1ΔUBD2-HA
Plasmid
GFP-Ub
doa4Δ
bro1Δ
Cells

SUPPLEMENTAL FIGURE LEGENDS

Figure S1-*related to Figure 1*. Effect Bro1 and ESCRT mutations

A. Lineage of *hse1*Δ cells used in genome sequencing experiments to determine the genetic basis for how loss of Hse1 results in a class E phenotype in SF838-9D parental background but not SEY6210. A sorting-defective haploid progeny from the SEY6210/SF838 *hse1*Δ homozygous diploid was backcrossed to the SEY6210 *hse1*Δ strain 2 times. Genomic DNA sequences from the indicated haploid progeny (samples 2 and 3) were compared with the SEY6210 *hse1*Δ strain. A search for ORF mutations common in samples 2 and 3 but not in sample 1 (Venn diagram) identified a difference in the *BRO1* open-reading frame.

B. Wildtype (WT) cells, or cells lacking *BRO1* (*bro1*Δ) or both *BRO1* and *HSE1* (*bro1*Δ *hse1*Δ) were transformed with plasmids expression Ste3-GFP, Ste3-GFP-Ub, or Mup1-GFP. Cell lysates were immunoblotted with α-GFP antibodies to reveal a vacuolar-processed form of GFP (GFP*).

C. Immunoblot (α-HA) of cells with the indicated genotype transformed with low-copy plasmid expressing Bro1-HA from the *BRO1* promoter (left). Bro1-HA was expressed to similar levels in all cell types (arrowhead). The non-specific band (*) serves as a loading control. Anti-Vps27 immunoblots of the cells with the indicated genotype (right). Vps27 (arrowhead) was expressed at similar levels in all cell types. The non-specific bands (*) serve as a loading control.

Figure S2-*related to Figure 2*. Comparison of *S castelli* and *S. cerevisiae* V domains

A. Sequence alignment of V domains from *S. castelli* and *S. cerevisiae*. Predicted α-helical regions are depicted. Boxed region describes a consensus clathrin binding box that is conserved in the Bro1 orthologs of other fungi. Residues identical between *S. cerevisiae* and *S. castelli* are blue, those identical between *S. cerevisiae, S. castelli, Kluyveromyces lactis, Pichia pastoris,* and *Candida dubliniensis* have an asterisk

B. Schematic of two arms of the Bro1 V domain and the position of the clathrin box within the predicted hinge region. Shown below is a sequence comparison of the clathrin box region amongst the indicated Bro1 orthologues.

C. Immunoblots (α-HA and α-PGK) of cells expressing the indicated HA epitope-tagged DUb fusion proteins used in Fig. 2

Figure S3-*related to Figure 3*. Binding of Ub by the first arm of Bro1.

A. Chemical shift perturbations of the backbone amides of ^{15}N-Ub (30μM) in the presence of 240μM *S. castelli* Bro1 V domain were calculated using the equation: $(0.2\Delta N^2 + \Delta H^2)^{1/2}$. Changes exceeding 1 S.D. above the mean for all perturbations (red line) were designated as most significant. Ten standard deviations above the mean chemical shift perturbations calculated from multiple experiments with ^{15}N-Ub alone is shown as a blue line indicating the threshold for measuring a chemical shift change.

B. Chemical shift perturbations of 30μM ^{15}N-Ub in the presence of 30μM Alix V domain.

C. Relative HSQC peak intensities averaged for residues 18 and 27 of ^{15}N-Ub (30μM) in HSQC experiments in the presence of increasing concentrations of indicated V domains.
D. Schematic of the half-V protein containing the helical regions comprising the first trihelical bundle that joins residues 370-410 to 529-646 of *S. castelli* Bro1 with an intervening SDG residue linker.
E. Residues comprising the half-V proteins (described in D) that are visible in the *S. castelli* V domain crystal structure are colored.
F. SDS-PAGE of purified half-V protein.
G. GST-pulldown of the half-V protein incubated with GST alone (ø) or GST fused to Ub, a mutant Ub (ub*), a tandem concatamer of 5 linear Ubs (5xUb), or Ub with a small 8 residue C-terminal extended tail (Ub^T).
H. Significant chemical shift perturbations induced on ^{15}N-Ub in NMR HSQC experiments in the presence of the mini-V protein were mapped onto the molecular surface of Ub.
I. Chemical shift perturbations (highlighted in H) of 30μM ^{15}N-Ub in the presence of 120 μM half-V were calculated using $(0.2\Delta N^2 + \Delta H^2)^{1/2}$. CSPs of 1 S.D. above the mean (red line) were plotted in H.

Figure S4-*related to Figure 4*. Position of Ub on *S. castelli* Bro1 V domain
A. Overlay of the two Bro1 V domain structures from Chain A (black) and Chain B (grey) found in the asymmetric unit. Superimposition was performed across all residues, yielding an RMSD of 4.022 for 285 aligned Cα atoms. Right shows closer view of superimposed V domains where Ub (green) is bound to Chain A.
B. Electron density maps shown at 1σ. Selenomethionines are shown as spheres, Chain B is grey, Chain A is colored according to amino acid order (blue-to-red).
C. PRE experiment using ^{15}N-Ub and MTSL-labelled Bro1 V at position 370, 381, and 392 in the N-terminus of the V domain (1:4). Left: Peak intensity ratios (oxidized vs. reduced spin label) for each Ub residue were calculated from HSQC spectra collected in the absence and presence of 2 mM ascorbate. The degree of PRE effect experienced by each Ub backbone amide is color-coded as indicated. These data were used to calculate an index of Differential PRE effect to compare relative distances of Ub backbone amides with spin labels placed at either residue 370 or 381. For each Ub residue, the PRE effect from labeling residue 370 was divided by the effect from labeling residue 381. Values <0.7 are colored orange, values >1.3 are colored green, all other values (equivocal) are grey. Thus, Ub residues assigned orange had a larger PRE effect with residue 370 of Bro1 V spin-labelled, and residues assigned green had a larger PRE effect with residue 381 spin-labelled. Right: Cartoon of Ub in a complex with the Bro1 V domain with residues undergoing differential PRE effect shown according to the color scheme. The positions of Bro1 V residues 370, 381, and 392 are indicated with spheres.

Figure S5-*related to Figure 5*. Bro1 V domain behaves as a larger protein in solution.
Scattering curves (**A**) and corresponding Guinier plots (**B**) of SAXS data collected for *S.castelli* Bro1 V and human Alix V domains. The linear fit of the Guinier plot is shown in

red. Also shown in A are the theoretical SAXS profiles for the open and closed forms of Alix and Bro1 V domains. Also shown is the profile of the optimum mix of open vs closed forms that best fit the experimental data. The quality of fit to experimental data ($\chi 2$), is shown for each profile.
C. Superdex 75 gel filtration purification profile and SDS-PAGE analysis of the major peak of Alix V domain.
D. Superdex 75 gel filtration purification profile and SDS-PAGE analysis of the major peak of *S. castelli* V domain.
E. Analysis of purified *S. castelli* Bro1 V and human Alix V domains by dynamic light scattering (DLS), gel filtration, static light scattering (SLS), as compared to the predicted molecular weight calculated by primary sequence.
F. Superdex 75 gel filtration profile and SDS-PAGE analysis of TEV-cleaved *S. castelli* Bro1 V^T domain. A TEV recognition site was introduced into the V domain by inserting ENLYFQ between residues 531 and 532. By SDS-PAGE intact Bro1 V was a single band at 37 kDa (lane 1) and cleaved to two bands of similar molecular weight by TEV protease (lane 2). TEV-cleaved Bro1 V was incubated at 25°C for 12 hrs before purification by gel-filtration over superdex 75; the peak fraction corresponding to apparent molecular weight of 60 kDa was analyzed by SDS-PAGE (lane 3).

Figure S6-*related to Figure 6*. Proton spectra of mutant Bro1 V domains.
One dimensional ^{1}H spectra of mutant V domains (90μM) in the presence of Ub (30μM) as compared to Ub alone (30μM).

Figure S7-*related to Figure 7*. Bro1$^{\Delta UBD1}$ and Bro1$^{\Delta UBD2}$ Sort Vacuolar Hydrolases
A. Expression levels of HA-tagged chimeric Bro1 containing the WT and mutant V domains from *S. castelli* are equivalent and similar to HA-tagged *S. cerevisiae* full-length Bro1. Shown are α-HA and α-PGK immunoblots of lysates from cells of the indicated genotypes transformed with the indicated plasmids.
B. CPY secretion was measured by growing cells on plates overlayed with nitrocellulose, which was removed after overnight growth and immunoblotted with α-CPY.
C. Distribution of GFP-Ub in cells with the indicated phenotype and carrying vector, WT *BRO1* or mutant *bro1* on low copy plasmid. Loss of Doa4 causes hyperaccumulation of GFP-Ub in the vacuole, loss of Bro1 function results in the accumulation of GFP-Ub on enlarged “class E” late endosomes.

Table S1. Plasmids used in this study.

Relevant to Figures 1-7

Plasmid	Description	Notes	Reference
pRSUb	Expression plasmid for human ubiquitin		Larsen, C.N.et al.,1996
pPL4466	mutant ubiquitin $A_{28}M$ in pRSUb		Pashkova et al, 2010
pPL2171	Ub-GST		Pashkova et al, 2010
pPL3894	ub*-GST		Pashkova et al, 2010
pPL3321	GST-Ub_tail		Pashkova et al, 2010
pPL3968	V5-5xUb		Pashkova et al, 2010
pET151	T7-6xHIS-V5 bacterial expression plasmid		Invitrogen
pPL4443	*S.castelli* Bro1 V residues 370-708 in pET151		This study
pPL4445	*S.cerevisiae* Bro1 V residues 372-703 in pET151		This study
pPL4609	*S.micatae* Rim20 V residues 339-656 in pET151		This study
pPL4611	*S.castelli* Rim20 V residues 352-676 in pET151		This study
pPL4612	*S.cerevisiae* Rim20 V residues 339-657 in pET151		This study
pPL4646	Human Alix V residues 360-713 in pET151		This study
pPL4648	*Pichia pastoris* Bro1 V residues 406-769 in pET151		This study
pPL4650	*Pichia pastoris* Rim20 V residues 220-529 in pET151		This study
pPL4672	Human HD-PTP V residues 361-711 in pET151		This study
pPL4778	*S.castelli* Bro1 V K417A, K418A, K419A in pET151	SEM	This study
pPL4782	*S.castelli* Bro1 V with TEV cleavage site at E532		This study
pPL4781	*S.castelli* Bro1 V C516N N517D D518N in pPL4443		This study
pPL4813	*S.castelli* Bro1 V E381C in pET151	a	This study
pPL4814	*S.castelli* Bro1 V N414C in pET151	a	This study
pPL4815	*S.castelli* Bro1 V N453C in pET151	a	This study
pPL4816	S.castelli Bro1 V E499C in pET151	a	This study
pPL4817	S.castelli Bro1 V A510C in pET151	a	This study
pPL4818	S.castelli Bro1 V E569C in pET151	a	This study
pPL4819	S.castelli Bro1 V D579C in pET151	a	This study
pPL4820	S.castelli Bro1 V S608C in pET151	a	This study
pPL4821	S.castelli Bro1 V S629C in pET151	a	This study
pPL4822	S.castelli Bro1 V T645C in pET151	a	This study
pPL4823	S.castelli Bro1 V Q655C in pET151	a	This study
pPL4824	S.castelli Bro1 V S680C in pET151	a	This study
pPL4901	S.castelli Bro1 V S392C in pET151	a	This study
pPL4902	S.castelli Bro1 V S442C in pET151	a	This study
pPL4903	S.castelli Bro1 V S463C in pET151	a	This study
pPL4904	S.castelli Bro1 V A489C in pET151	a	This study
pPL4905	S.castelli Bro1 V S551C in pET151	a	This study
pPL4906	S.castelli Bro1 V S598C in pET151	a	This study
pPL4907	S.castelli Bro1 V S702C in pET151	a	This study
pPL4941	S.castelli Bro1 V I371R Y372A in pET151	a,b	This study
pPL4978	S.castelli Bro1 V S376A I377A Y378A in pET151	a,b	This study
pPL4979	S.castelli Bro1 V Y378A S379A E380A in pET151	a,b	This study
pPL4980	S.castelli Bro1 V S379R A383R in pET151	a,b	This study
pPL4981	S.castelli Bro1 V I377R in pET151	a,b	This study
pPL4982	S.castelli Bro1 V Y378R in pET151	a,b	This study
pPL4983	S.castelli Bro1 V L385R in pET151	a,b	This study
pPL4984	S.castelli Bro1 V L386R in pET151	a,b	This study
pPL4985	S.castelli Bro1 V S376R in pET151	a,b	This study
pPL4986	S.castelli Bro1 V E394R in pET151	a,b	This study
pPL4987	S.castelli Bro1 V L385N L386N in pET151	a,b	This study
pPL4988	S.castelli Bro1 V M390 E391N in pET151	a,b	This study
pPL4989	S.castelli Bro1 V K578E in pET151	a,b	This study
pPL4990	S.castelli Bro1 V F625R in pET151	a,b	This study
pPL4991	S.castelli Bro1 V E621R in pET151	a,b	This study
pPL4992	S.castelli Bro1 V F606D in pET151	a,b	This study
pPL5052	S.castelli Bro1 V I377R E380A in pET151	a,b	This study
pPL5053	S.castelli Bro1 V I377R L386R in pET151	a,b	This study
pPL5054	S.castelli Bro1 V E380A L386R in pET151	a,b	This study
pPL5055	*S.castelli* Bro1 V E370C in pET151	a	This study

pPL5056	*S.castelli* Bro1 V E373C in pET151	a	This study
pPL5057	*S.castelli* Bro1 V L386A in pET151	a,b	This study
pPL5060	S.*castelli* Bro1 V I377A E380R in pET151	a,b	This study
pPL5061	*S.castelli* Bro1 V I377A E380R L386A in pET151	a,b	This study
pPL4945	*S.castelli* Bro1 V R387E K388E in pET151	a,b	This study
pPL4946	*S.castelli* Bro1 V E389A M390A E391A in pET151	a,b	This study
pPL4948	*S.castelli* Bro1 V R564D K567D in pET151	a,b	This study
pPL4950	*S.castelli* Bro1 V L566A K567A E568A in pET151	a,b	This study
pPL4951	*S.castelli* Bro1 V K567A E568A E569A in pET151	a,b	This study
pPL4953	*S.castelli* Bro1 V R572A T573A M574A in pET151	a,b	This study
pPL4959	*S.castelli* Bro1 V T617A T618A R619A in pET151	a,b	This study
pPL4955	*S.castelli* Bro1 V L605A F606A E607A in pET151	a,b	This study
pPL4957	*S.castelli* Bro1 V L610A K612E in pET151	a,b	This study
pPL4993	*S.castelli* Bro1 V (370-410-SGD-529-646) in pET151	1/2 V	This study
pPL4469	Mouse Cks1 in pET151		This study

pRS315, pRS316	LEU2 and URA3 yeast expression plasmids	Sikorski, R.S. & Hieter, P.,1989
pPL967	Ste3-GFP in pRS315	Urbanowski and Piper, 2001
pPL2089	Sna3-GFP in pRS315	Stringer and Piper, 2011
pPL3791	*CUP1* promoter Gap1-GFP in pRS315	Stringer and Piper, 2011
pPL3797	*CUP1* promoter Fur4-GFP in pRS315	Stringer and Piper, 2011
pPL3878	GFP-Ub in pRS315	Ren and Piper, 2007
pPL4069	Mup1-GFP in pRS315	Stringer and Piper, 2011
pPL4148	*CUP1* promoter HIS3-UL36-3xHA	Stringer and Piper, 2011
pPL4178	*CUP1*promoter Bro1-HA from *S.cerevisiae*	This study
pPL4256	*S. cerevisiae* Bro1 V residues 372-703 in pGEX-6P-1	This study
pPL5025	chimeric Bro1-2xHA with V domain from pPL4781	This study
pPL5026	chimeric Bro1-2xHA with V domain from pPL4984	This study
pPL5034	chimeric Bro1-2xHA with V domain from pPL4445	This study
pPL5059	chimeric Bro1-2xHA with V domain from pPL4981	This study
pPL5073	Bovine clathrin (1-163) NTD-NEMO in pET28a	Linton Traub
pPL5074	Yeast clathrin (1-163) NTD in pET28a	Linton Traub
pPL5079	*CUP1* promoter Bro1-UL36-3xHA in pRS316	This study
pPL5080	*CUP1* promoter Bro1-Ubp7-3xHA in pRS316	This study
pPL5099	*CUP1* promoter BroDomain-UL36-3xHA in pRS316	This study
pPL5113	*CUP1* promoter MIT-UL36-3xHA in pRS316	This study

List of plasmids that includes the plasmid name, the relevant contents of the plasmid and the study that produced the plasmids
The Notes section desginates the following:
a - has C516N N517D D518N substitutions
b - has E381C substitution
SEM - Surface Entropy Minimization

Table S2. Yeast strains used in this study

Relevant to Figures 1, 2 and 7

Strain	Genotype	Source
SF838-9D	*MATα leu2-3,112 ura3-52 his4-519 ade6 pep4-3*	Raymond et al., 1992
SEY6210	*MATα leu2-3,112 ura3-52 his3-Δ200 trp1-Δ901 lys2-801 suc2-Δ9 mel*	Robinson et al., 1988
PLY3095	*SF838-9D; PEP4 hse1Δ::KanR*	This Study
EE10	*SEY6210; MATa*	Scott Moye-Rowley, U of Iowa
PLY3091	*SEY6210(EE10) MATa hse1Δ::TRP1*	This Study
PLY4249	*SEY6210(EE10) MATa hse1Δ::TRP1 bro1Δ::URA3*	This Study
PLY4259	*SF838-9D; PEP4 hse1D::KanR bro1Δ::URA3*	This Study
PLY3418	*SEY6210; vps27-ΔCHC::TRP1::GAL1-VPS27*	Bilodeau et al., 2003
PLY3912	*SEY6210; hse1Δ::KanR*	Stringer and Piper, 2011
PLY3951	*SEY6210; vps23ΔUb(F52Q117W125) VPS36::TRP1::vps36Δ::NAT*	Shields and Piper, 2009
PLY4225	*SEY6210; bro1Δ::lox-HIS5-lox*	This Study
PLY4229	*SEY6210; bro1Δ::lox-HIS5-lox hse1Δ::KanR*	This Study
PLY4230	*SEY6210; bro1Δ::lox-HIS5-lox, vps23ΔUb(F52Q117W125)*	This Study
PLY4246	*SEY6210; bro1Δ::lox-HIS5-lox vps27ΔCHC::TRP1::GAL1-VPS27*	This Study

List of yeast strains that includes the yeast strain name, the relevant genotype and the source, which describes the studies where the strain was initially made.

Movie Legend- *Relevant to Figure 5.*
Animation emphasizing the conformational changes between the “closed” form of Alix V (PDB:2OEX) and the “open” form of Alix V (PDB ID: 4JJY) that were determined here and previously by Xray crystallography.

EXPERIMENTAL PROCEDURES

Fragments encoding V-domains were amplified by PCR from genomic DNA of *S. cerevisae*, *S.castelli*, *S.micatae*, or obtained by gene synthesis (Genscript, Piscataway, NJ) and subcloned into pET151/D-TOPO (LifeTechnologies, Carlsbad, CA). Point mutations were generated by QuickChange mutagenesis (Agilent Technologies, Santa Clara, CA). Yeast *BRO1*-expressing plasmids cells with various V-domains were made by homologous recombination into BglII digested low copy/CEN plasmid encoding the flanking N-terminal and C-terminal portions of *S. cerevisiae* Bro1 upstream of a 2x-tandem HA epitopes all driven by the *BRO1* promoter.

Antibodies used: α-Ub monoclonal antibody P4D1 (Santa Cruz Biotechnology Inc., Santa Cruz, CA); polyclonal α-V5 and α-HA (QED Bioscience Inc., San Diego, CA); monoclonal α-V5 (Life Technology, Calrsbad, CA), monoclonal α-HA (Covance Research Products Inc.,Berkley, CA); monoclonal α-His Tag antibody (GenScript, Piscataway, NJ); polyclonal α-Vps27 and monoclonal α-CPY and α-PGK1 (Tom Stevens, University of Oregon); monoclonal α-Chc1 (Sandra Lemmon, University of Miami).

N-terminally 6X-His tagged Alix V and Bro1 V domains were in produced in *E.coli* BL21(DE3) cells induced with 0.5 mM IPTG at 20°C for 18hrs, purified over TALON Co^{2+} affinity resin (Clontech, Mountain View, CA) and eluted in 287mM NaCl, 2.7mM KCl, 12mM $NaPO_4$, 150mM imidazole, pH 7.7. For crystallization, V-domains were cleaved from 6xHis tag with TEV protease and purified by size exclusion chromatography on a HiLoad 16/60 Superdex 200 column (GE Healthcare Biosciences, Pittsburg, PA) in 20 mM Hepes pH 7.4, 100mM NaCl. SeMet-labelled proteins were expressed using a methionine pathway inhibition procedure in which cells were grown in LB to OD_{600} of 0.8/ml, washed and resuspended in M9 minimal media containing 0.5% glucose, 50mg/l leucine, isoleucine and valine, and 100 m/l phenylalanine, lysine, and threonine. Cells were grown for 20 min before the addition of 50mg/l seleniomethionine and IPTG. Wild-type and SeMet-Ub(A_{28}M) was expressed from pRSUb by transforming into BL21 cells and growing transformants in media with 0.5% glucose and 25µg/ml ampicillin prior to dilution in LB and induction in IPTG. Ubiquitin was purified from bacterial lysates adjusted to 3.5% perchlorate; Ub in the soluble fraction was dialyzed and purified over cation exchange chromatography.. Complexes of Bro1V:Ub and AlixV:Ub at 13-25 mg/ml were made by combining V domain proteins with wild-type or A_{28}M Ub at a 1:1.5 molar ratio in 20mM HEPES pH 7.4, 100mM NaCl buffer at 4°C.

Crystals containing Bro1V were grown at 18°C by mixing equal amount of the protein samples and solution containing 0.1M bis-Tris propane pH 7, 0.2-0.4M Na malonate, 15-20% PEG 3350. Bro1V:Ub (A28M) crystals grew by the hanging drop method for 2-3 weeks as thick rods and were used to collect X-ray diffraction data to 3.5 Å. To improve the quality of crystals with SeMet-Bro1V crystals, K417A, K418A, K419A mutations were made to reduce surface entropy (http://services.mbi.ucla.edu/SER/). Diffraction quality crystals grew after a month at 18°C as short rods and were used to collect a 3.5 Å SAD dataset. All crystals were flash cooled in liquid N_2 directly from crystallization solution. AlixV:Ub crystals were grown at 4°C by mixing equal amount of the protein sample and solution containing 0.1 M Na citrate pH 5, 6-8 % PEG 8000, 5-10% ethylene glycol. Cubic crystals appeared within a week and grew to full size in 7-10 days. Prior to flash cooling in liquid nitrogen, AlixV:Ub crystals were cryoprotected in a reservoir solution supplemented with 20% ethylene glycol. Diffraction data were collected at 100 K on the 4.2.2 beamline at the Advanced Light Source (Berkeley, CA) at 12700 eV. Crystallization of AlixV or Bro1V(K417A, K418A, K419A) with SeMet-Ub(A28M) gave poor quality crystals that diffracted to only 7-8 Å. After the crystals were back-soaked in the crystallization well solution, a strong anomalous signal from scanning at the Selenium edge confirmed presence of SeMet-Ub in both crystals.

The diffraction data for SeMet-Bro1V:Ub (A28M) were processed using d*TREK (Pflugrath, 1999) and phased with phenix.autosol (Terwilliger et al., 2009) using the SAD method. All 10 Selenium sites (2 Bro1V molecules in the asymmetric unit) were located and one of the two hands after phasing showed clear tubular electron density representing the arms of the Bro1V. Phenix.autobuild and phenix.refine were used to iteratively build and improve the Bro1V model. Ub (pdb id: 1UBQ) was then docked into the clearly visible density near the Bro1V N-terminus and refined. Since side-chains could not be clearly modeled at this resolution, most of the residues in the model were trimmed to the C_β atom. The diffraction data for SeMet-AlixV:Ub were integrated and scaled using d*TREK and prepared for SHELXD using xprep. All 10 Selenium sites (2 AlixV molecules in the asymmetric unit) could be located and density modification/backbone tracing using SHELXE gave an interpretable map for one of the two hands. Phenix was used to improve the quality of the map sufficiently such that the two arms of AlixV from the high-resolution structures could be chopped at the hinge region, independently placed in the electron density and then refined. Coot and PyMOL were used to manually fit the structure and generate the structural figures.

SAXS data (collected at the 12-ID-B beamline at the Advanced Photon Source, Argonne National Laboratory) from 20µl samples of Alix and Bro V domains at concentrations ranging from 1 to 10 mg/ml at 20°C and exposure times of 1, 2 and 4 s were used to establish concentration dependence on scattering and exposure based radiation damage. The final SAXS dataset was collected at the SIBYLS 12.3.1 beamline at the Advanced Light Source (Lawrence Berkeley National Laboratory) at 10°C on samples ranging in concentration from 1 to 6 mg/ml and exposure times of 0.5, 1, 2 and 4s. Data were processed with PRIMUS (Konarev et al., 2003) after correction with matching buffers. The radius of gyration (Rg) estimated from the linear region of the Guinier plots was 34.3 Å for Alix V and 35.4 Å for Bro1 V. A pair distance distribution P(r) function was calculated using GNOM to estimate of the maximum dimension (D_{max}) of the V domains and yielded values of 116.0 Å and 111.1 Å for Alix and Bro1 V domain respectively. The *ab initio* models using a chain-like ensemble of dummy residues were generated with GASBOR (Svergun et al., 2001). Theoretical SAXS profiles of open and closed V ensembles were generated with FoXS and its Minimal Ensemble Search algorithm was used to calculate weighted fit of the open and closed forms of V domains (Schneidman-Duhovny et al., 2010).

^{15}N-HSQC spectra were collected at 25°C on a Bruker Avance II 800 MHz spectrometer using 30µM ^{15}N-labelled Ub in 50mM NaCl, 40mM NaPO4, pH 6.95. Data were analyzed with SPARKY (T. D. Goddard and D. G. Kneller, SPARKY 3, UCSF, CA) and NMRView (One Moon Scientific, Westfield, NJ). Chemical shift perturbations were measured by comparing peak positions to ^{15}N-Ub alone using $(0.2*\Delta ppmN^2 + \Delta ppmH^2)^{1/2}$). Paramagnetic relaxation enhancement effects were measured using a series of cysteine-containing mutants of Bro1 V domain labeled with the paramagnetic spin label MTSL [(1-oxyl-2,2,5,5-tetramethylpyrroline-3-methyl) –methanethio- sulfonate] purchased from TRC Inc. (Toronto, Canada). Incorporation to >90% was validated by electron spin resonance analysis. Two ^{15}N/^{1}H HSQC spectra of ^{15}N-Ub were acquired when complexed with each spin-labeled Bro1 V sample: one spectrum for the sample having the MTSL spin-label in the oxidized (paramagnetic) state and 2nd spectrum for the duplicate sample containing 2mM ascorbate which reduced MTSL to the diamagnetic state. The peak intensity ratios of the oxidizied vs. reduced samples were calculated and served as a means to quantify the degree of PRE effects (e.g. a lower peak intensity ratio reflecting a larger PRE effect experienced by the particular crosspeak or residue of Ub).

Cells expressing GFP-fusion proteins were grown to mid-log phase in Synthetic Dextrose (SD) minimal media at 30°C. Genes under control of the *CUP1* promoter were induced with the addition of 50µM $CuCl_2$. Cells were resuspended in 0.2% NaN_3, 100mM Tris pH 8.0 before imaging by epifluorescence using an Olympus BX60 equipped with 1.4 N.A.100x objective and an Orca R2 CCD camera (Hamamatsu Photonics, Bridgewater, NJ). Images were collected with iVision software (Biovision Technology, Exton, PA) and processed in Adobe Photoshop.

Yeast protein extracts for SDS-PAGE and immunoblotting were prepared by resuspending cell pellets in 0.2M NaOH for 1 min followed by repelleting and resuspending in 20 mM Tris pH 6.8, 5% SDS, 8M urea, 10% glycerol. Immunoblots were visualized by chemilumenescence with HRP-conjugated secondary antibody (GE Healthcare Biosciences, Pittsburg, PA) or fluorescence with IRDye-conjugated secondary antibody (Li-COR Biosciences, Lincoln, Nebraska).
GST pull-down experiments were done using 150µg of GST or GST fusion proteins attached to 50µls GSH beads mixed with the lysates of bacteria or yeast cells expressing input proteins. Beads and input proteins, either purified or as cell lysates, were incubated in a total volume of 700 µls PBS containing 0.1 mg/ml BSA, 0.01% Triton X-100 with gentle agitation for 1 hr at 25°C. Beads were washed 3 times in PBS (4°C) and bound complexes were eluted with 50 µls of PBS containing 50mM reduced glutathione. Samples were diluted with 5% SDS, heated, and subjected to SDS-PAGE and immunoblotting.

For immunoprecipitation, yeast lysates prepared from spheroplasts were incubated with IgGSorb beads precoated with polyclonal anti-HA antibodies for 1 hr on ice in PBS pH 7.4 containing 0.02% Trition X100, 0.1% BSA, 1 mM EDTA, and protease inhibitors in 200 µl. Binding to K63 polyubiquitin was done by attaching recombinant 6xHis-V5-tagged V-domains to 30µls of beads coated with polyclonal anti-V5 antibodies, which were subsequently incubated for 1 hr with 2 µg of K63-linked polyUb (Boston Biochemicals, Cambridge, MA) in 200µl PBS containing 0.02% of Trition X100, 0.1% BSA or casein. Beads were washed 5 times; bound complexes were eluted with Laemmli sample buffer and heating to 70°C for 5 min.

To measure CPY secretion, cells transformed with *BRO1-HA* plasmids were grown to OD=2 and plated as 3 µl drops and incubated for 18 hrs at 30°C after overlay with nitrocellulose membrane, which was immunoblotted using anti-CPY antibody.

To compare yeast genomic DNA, 7-9 million 75 base-pair, single-end reads were generated for each sample on an Illumina HiSeq 2000 platform machine (San Diego, CA). Prior to mapping, trailing bases noted as of poor quality through the use of the Read Segment Quality Control Indicator of 'B' were converted to 'N'. Reads were mapped to the sacCer3 genome (UCSC Genome Bioinformatics Group) using the BWA alignment program without additional options (Li and Durbin, 2009). PCR/optical duplicates were filtered out using Picard (sourceforge.net) and reads were further filtered to exclude non-uniquely mapping reads and for reads in Samples #2 and #3 to exclude reads with a quality score of less than 30 (q<30). The samtools mpileup program (Li et al., 2009) was used to call single nucleotide variants; the samtools -C 50 filter was applied to Samples #2 and #3 but not to Sample #1. We applied the vcfutils.pl varFilter to the raw .bcf file generated by mpileup using a value of –D 100, which is greater than twice the average coverage of each sample. Insertions and deletions were called with the Genome Analysis Tool Kit after local realignment (DePristo et al., 2011; McKenna et al., 2010). Custom python scripts, including a mutation annotation script (http://depts.washington.edu/sfields/software/annotate/), identified 26 genic or 5'-upstream mutations that were shared between Samples #2 and #3 but were absent from Sample #1; one of these was a G to A transition resulting in the *BRO1* C359Y mutation. No aneuploidy or unique copy-number variants were detected in Samples #2 or #3 as assessed by determining the average coverage in 100 base-pair non-overlapping windows for each sample as calculated by IGVtools (Broad Institute, MA) combined with manual examination of the most extreme regions of copy-number change.

Supplemental References

Bilodeau, P.S., Winistorfer, S.C., Kearney, W.R., Robertson, A.D., and Piper, R.C. (2003). Vps27-Hse1 and ESCRT-I complexes cooperate to increase efficiency of sorting ubiquitinated proteins at the endosome. J Cell Biol *163*, 237-243.

DePristo, M.A., Banks, E., Poplin, R., Garimella, K.V., Maguire, J.R., Hartl, C., Philippakis, A.A., del Angel, G., Rivas, M.A., Hanna, M.*, et al.* (2011). A framework for variation discovery and genotyping using next-generation DNA sequencing data. Nat Genet *43*, 491-498.

Konarev, P., Volkov, V., Sokolova, A., Kocj, M., and Svergun, D. (2003). PRIMUS: a Windows PC-based system for small-angle scattering data analysis. J Appl Cryst *36*, 1277-1282.

Larsen, C.N., Price, J.S., and Wilkinson, K.D. (1996). Substrate binding and catalysis by ubiquitin C-terminal hydrolases: identification of two active site residues. Biochemistry *35*, 6735-6744.

Li, H., and Durbin, R. (2009). Fast and accurate short read alignment with Burrows-Wheeler transform. Bioinformatics *25*, 1754-1760.

Li, H., Handsaker, B., Wysoker, A., Fennell, T., Ruan, J., Homer, N., Marth, G., Abecasis, G., and Durbin, R. (2009). The Sequence Alignment/Map format and SAMtools. Bioinformatics *25*, 2078-2079.

McKenna, A., Hanna, M., Banks, E., Sivachenko, A., Cibulskis, K., Kernytsky, A., Garimella, K., Altshuler, D., Gabriel, S., Daly, M.*, et al.* (2010). The Genome Analysis Toolkit: a MapReduce framework for analyzing next-generation DNA sequencing data. Genome Res *20*, 1297-1303.

Pashkova, N., Gakhar, L., Winistorfer, S.C., Yu, L., Ramaswamy, S., and Piper, R.C. (2010). WD40 repeat propellers define a ubiquitin-binding domain that regulates turnover of F box proteins. Mol Cell *40*, 433-443.

Raymond, C.K., Howald-Stevenson, I., Vater, C.A., and Stevens, T.H. (1992). Morphological classification of the yeast vacuolar protein sorting mutants: evidence for a prevacuolar compartment in class E vps mutants. Mol Biol Cell *3*, 1389-1402.

Ren, J., Kee, Y., Huibregtse, J.M., and Piper, R.C. (2007). Hse1, a component of the yeast Hrs-STAM ubiquitin-sorting complex, associates with ubiquitin peptidases and a ligase to control sorting efficiency into multivesicular bodies. Mol Biol Cell *18*, 324-335.

Schneidman-Duhovny, D., Hammel, M., and Sali, A. (2010). FoXS: a web server for rapid computation and fitting of SAXS profiles. Nucleic Acids Res *38*, W540-544.

Sikorski, R.S., and Hieter, P. (1989). A system of shuttle vectors and yeast host strains designed for efficient manipulation of DNA in Saccharomyces cerevisiae. Genetics *122*, 19-27.

Stringer, D.K., and Piper, R.C. (2011). A single ubiquitin is sufficient for cargo protein entry into MVBs in the absence of ESCRT ubiquitination. J Cell Biol *192*, 229-242.

Svergun, D.I., Petoukhov, M.V., and Koch, M.H. (2001). Determination of domain structure of proteins from X-ray solution scattering. Biophysical journal *80*, 2946-2953.

Urbanowski, J.L., and Piper, R.C. (2001). Ubiquitin sorts proteins into the intralumenal degradative compartment of the late-endosome/vacuole. Traffic *2*, 622-630.